PHOTOGRAMMETRIC MONITORING OF AN ARTIFICIALLY GENERATED SHALLOW LANDSLIDE

Devrim Akca* (akca@isikun.edu.tr)

Isik University, Istanbul, Turkey

Formerly at Swiss Federal Institute of Technology (ETH), Zurich

Abstract

An artificial rainfall event was applied to a forested slope in Ruedlingen, northern Switzerland. The experiment triggered a landslide which resulted in mobilising about 130 m^3 of debris. The event was monitored by a photogrammetric network of four cameras, operating at 5 to 8 frames per second, in order to quantify spatial and temporal changes by tracking tennis balls pegged into the ground. Image measurements were performed using automated image matching methods, implemented through a software package developed in-house. Three-dimensional coordinates of the target points were estimated by running a customised type of bundle adjustment, achieving a positioning precision of ± 1·8 cm.

KEYWORDS: bundle adjustment, camera synchronisation, high speed camera, landslide monitoring, network design, photogrammetric network simulation

INTRODUCTION

THE UNDERSTANDING OF LANDSLIDE mechanisms is greatly facilitated when information on their horizontal and vertical displacements is available (Dewitte et al., 2008). Geotechnical sensors, such as piezometers, inclinometers and extensometers, have been used to a great extent (Angeli et al., 2000; Ayalew et al., 2005; Corsini et al., 2005), although they only provide one-dimensional information.

Geodetic techniques can provide 2D and even 3D spatial information in point or surface form. Remote sensing satellite imagery (Metternicht et al., 2005; Martha et al., 2010; Lodhi, 2011; Debella-Gilo and Kääb, 2012), Global Positioning Systems (Malet et al., 2002; Mora et al., 2003), total stations (Petley et al., 2005), ground-based SAR interferometry (Tarchi et al., 2003), terrestrial laser scanning (Travelletti et al., 2008; Pesci et al., 2011), airborne laser scanning (Bell et al., 2012), unmanned aerial vehicles (Niethammer et al., 2012), airborne photogrammetry (Chadwick et al., 2005; Baldi et al., 2008; Dewitte et al., 2008) and high speed digital cameras (Dewez et al., 2010) have been utilised for the pre- and post-analysis of landslide events, risk assessment and long-term monitoring tasks.

A landslide event must be monitored by a measurement system operating at a very high data acquisition rate when a thorough understanding of landslide dynamics is being researched. Digital close range photogrammetry is an optimal solution for such missions in terms of data frequency, coverage, resolution and accuracy. Ochiai et al. (2004) monitored a landslide induced by artificial rainfall using close range photogrammetry. They determined the motion of the surface using five stereopairs from 10 low-resolution (640 × 480 pixels) CCD cameras.

Triggering of Rapid Mass Movements in Steep Terrain (TRAMM) is an inter-disciplinary project conducted by cooperation between the Swiss Federal Research Institute WSL, ETH Zurich and EPF Lausanne, Switzerland. The primary goal of the project is to improve the quantification and predictability of hazardous mass movements, including landslides, snow avalanches and debris flows. The project aims to conduct laboratory and field experiments, spatial analyses of hill-slope failures, the development of new modelling approaches and new measurement methodologies. The research tasks that are emphasised include the spatial characterisation of hazard-prone slopes, improved understanding of triggering mechanisms and mass dynamics.

The TRAMM project has six test sites. An artificial shallow landslide was generated at one of them near Ruedlingen, a small town in the north of Switzerland, and the mass dynamics were studied numerically. Parameters such as pore water pressure, volumetric water content, horizontal soil pressure, temperature, piezometric water level, and surface and subsurface deformations were monitored during the sprinkling experiment (Askarinejad et al., 2010; Springman et al., 2010).

This paper covers the details of the close range photogrammetric image data processing work of the Ruedlingen experiment. The goal of the photogrammetric work was to quantify the spatial and temporal changes in the landslide surface. Points were signalised with markers and their movement was tracked during the landslide, while their 3D coordinates were estimated at each instant of image acquisition. The photogrammetric work provided input to the geotechnical analysis for a better understanding of the landslide's characteristics, and also provided external data for the validation of other field instruments.

The first sprinkling experiment was conducted in the autumn of 2008, in which a failure did not occur. Subsequently, a second experiment was planned and executed in the spring of 2009 which did result in a landslide. In a previous publication (Akca et al., 2011) the characteristics of the test site, the workflow and the numerical results of both sprinkling experiments were discussed. This paper focuses on the second experiment and emphasises the computational and algorithmic details of the photogrammetric work.

The next section introduces the test site area. The following section provides details of the experiment. The photogrammetric network design, network simulation, equipment and installation, camera calibration, image orientation, target tracking and point positioning with aspects of the bundle adjustment are explained in detail.

Test Site in Ruedlingen

The test site is located on a steep slope next to the River Rhine near Ruedlingen, northern Switzerland (Fig. 1). The test area is about 10 m by 35 m in size and has an average slope of 38° (Fig. 2). The ground was cleared of trees and bushes prior to the experiment.

Ruedlingen was chosen following an extreme event in May 2002 in which 100 mm of rain had fallen in 40 min, leading to 42 landslides around the local area (Springman et al., 2010).
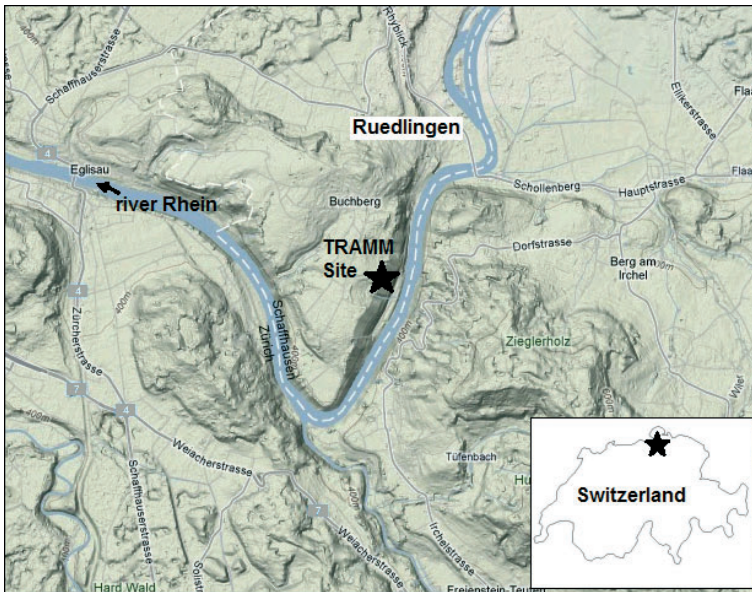
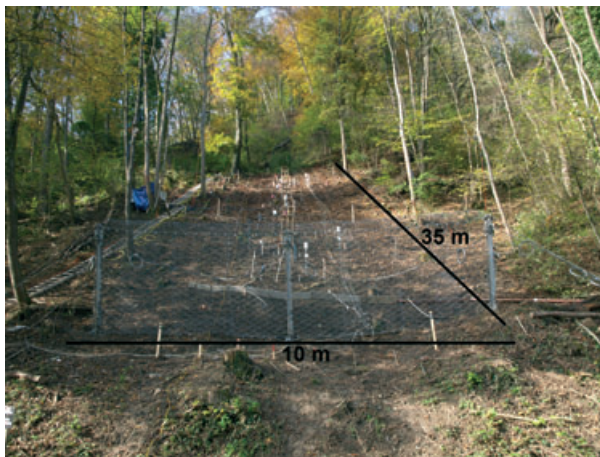Fig. 1. The TRAMM test site near Ruedlingen, Switzerland.

Fig. 2. The test site has dimensions of 10 m by 35 m.

THE RUEDLINGEN EXPERIMENT

After identification of a possible steep slope that would be susceptible to a shallow landslide on the basis of geology, topography, accessibility, vegetation and expected ground profile, the layers of soil and depth to the underlying rock were determined to decide whether the experiment would be feasible or not. A series of test pits were dug around the

edges of the projected testfield to determine soil layering, investigate the root systems, locate rock depth and extract soil samples.

Photogrammetric Network Design

Two tall trees beyond the experiment area on its lower side (shown as Tree1 and Tree2 in Fig. 3), both of which are approximately 25 m in height, were selected as positions for the cameras. A four-camera arrangement (two cameras per tree) was used to provide adequate photogrammetric coverage of the experimental area.

An initial map of the area (Fig. 3) was generated using total stations. This information served as input to a photogrammetric network simulation tool developed in-house, called PanCam. PanCam is a routine which can estimate the a posteriori point positioning precision provided that the input parameters of the designed photogrammetric network are given (Amiri Parian et al., 2007). The proper camera formats and lenses were interactively examined in the simulation environment. The network design and simulation steps are essentially required in order to predict the theoretical precisions of point coordinates (Saadatseresht et al., 2004; Olague and Dunn, 2007; Rieke-Zapp et al., 2009).

The sprinkling experiment aims to trigger a shallow landslide where the slow mobilisation of the mass is followed by a sudden movement downhill. Therefore, a high-speed set of cameras which has a continuous day and night coverage capability must be used. Accordingly, 1·3 megapixel IDS uEye UI-6240 C video cameras (IDS – Imaging Development Systems, Obersulm, Germany) were chosen for the image acquisition (Fig. 4). Technical details of the cameras are given in Table I. Intentionally, a CCD type of sensor was preferred over the CMOS sensors since radiometric quality is a concern, especially for the night-time images.

Using the PanCam tool, the a priori point positioning accuracy of the signalised targets was estimated to be ±12·4 mm in the horizontal direction and ±4·2 mm in the vertical direction (Fig. 5). The a priori standard deviation of the image point observations was assumed to be ±0·1 pixel. The design consideration for the project is to track the points during the landslide within a positional accuracy of ±1 to 2 cm. According to the
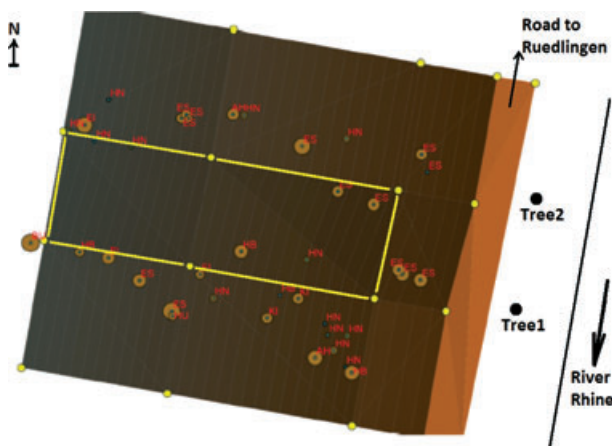

FIG. 3. The test site is delineated by yellow lines. Tree1 and Tree2 are located on the opposite side of the road to Ruedlingen.

TABLE I. Technical details of IDS uEye UI-6240 C video cameras.

	IDS UI-6240 camera
Sensor type	CCD
Sensor size	½ inch (12·7 mm)
Image format	1280 × 1024 pixels
Shutter	Global shutter
Frame rate	14 fps
Pixel pitch	4·65 μm
Data transmission protocol	Gigabit ethernet

FIG. 4. IDS uEye UI-6240 C gigabit ethernet video camera.

simulation results, the photogrammetric network, as designed, meets this requirement satisfactorily.

SET-UP PRIOR TO ARTIFICIAL RAINFALL

Equipment and Installation

The four IDS cameras were equipped with two 8·0 mm and two 12·0 mm C-mount lenses. The two cameras equipped with 8·0 mm lenses (CAM1 and CAM2 in Fig. 6) were directed towards the lower part of the experimental area and were located 13 m above the ground. The other two cameras, with 12·0 mm lenses (CAM3 and CAM4 in Fig. 6), were directed towards the upper part of the experimental area and were positioned 18 m above the ground. The baselines of the cameras were 5·1 m up and down the tree trunks, and 6·2 m between the two trees. This arrangement provided 100% imaging overlap with all four cameras.

The cameras were placed in housing shields (Fig. 7) which protected them against snow, rain, dust and other environmental effects. They were fixed on the trees by a professional climber.

All the cameras were connected to a central computer using approximately 100 m of Cat-6 ethernet cables. The control computer was a Fujitsi-Siemens Celsius W-360 PC with an Intel Core 2 Quad 2·4 GHz CPU, 4 GB DDR2 RAM, one 250 GB and two 500 GB 7200 rpm SATA II hard discs, and a MS Windows Server 2003 R2 Enterprise operating
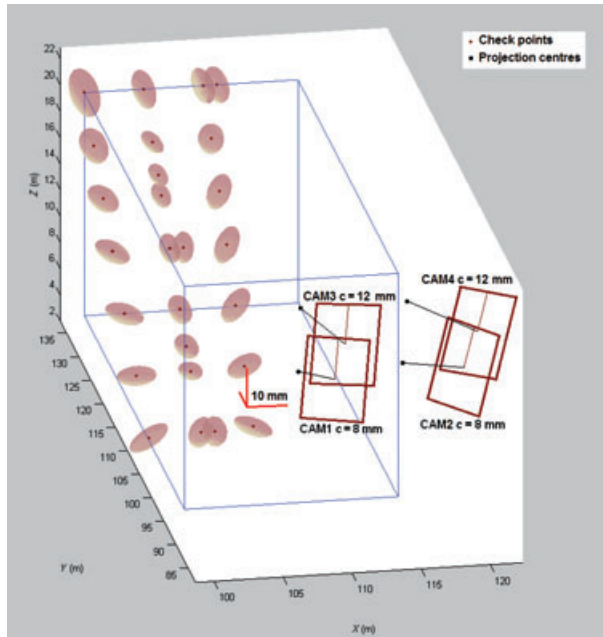
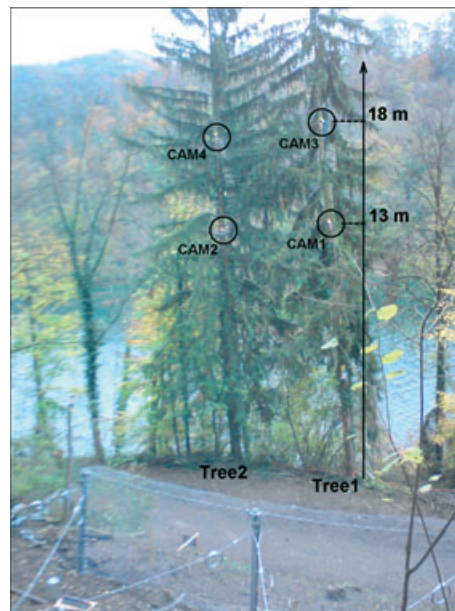Fig. 5. The a priori estimated error ellipsoids of some representative signalised targets.

Fig. 6. The four cameras were fixed on two trees at 13 and 18 m height.

FIG. 7. The cameras, placed in housing shields, were fixed on the trees by a climber.

system. An Intel Pro/1000 PT Quad Port Network Interface Card (NIC) was used for the ethernet protocol communication.

The cameras were set to operate at a data acquisition rate of 10 frames per second (fps). The imaging frequency of the four cameras was synchronised using in-house image acquisition software, which is a MS Windows multi-threading application, developed using the C# programming language and IDS SDK (Software Development Kit) library functions. Standard MS Windows software uses single-threading applications, where instructions are executed serially. Multi-threading is a software programming concept where multiple instructions can run synchronously in parallel. The in-house image acquisition software enables the four cameras to shoot (and store) the frames simultaneously. The multi-threading software approach has a synchronisation error of $\pm 2\,\mathrm{ms}$ in all cases. An alternative to software synchronisation is hardware synchronisation, where external triggers and additional synchronisation cables are employed; however, this approach would incur additional cost to the project budget.

The synchronisation of the cameras is extremely important when monitoring such dynamic events; otherwise, cheaper cameras with a larger image format could have been bought and would thus have obtained even better results.

Deformations were monitored during the experiment, both on the surface via the photogrammetric camera network and within the soil mass using a flexible probe. The latter was equipped with strain gauges at different points, two axis inclinometers on top and acoustic sensors. Other instruments were installed at depths of 15, 30, 60, 90, 120 and 150 cm below the ground surface over the slope; these included jet-fill tensiometers, time domain reflectometers (TDRs), Decagon TDRs, piezometers, soil temperature sensors, deformation probes, earth pressure cells, acoustic sensors and rain gauges (Springman et al.,

2010). A ring-net barrier (provided by Geobrugg, Romanshorn, Switzerland) was set up at the foot of the slope to protect the road (Figs. 2 and 6).

Signalised Targets

Seventy-six yellow tennis balls (80 mm diameter), glued to 25 to 35 cm wooden sticks, were used as the artificial targets. The sticks were pushed vertically into the ground in a regular grid arrangement. Thirteen of the tennis balls were occluded by a textile strip (right side of Fig. 9). The remaining 63 tennis balls were effectively used in the continuation of the experiment. The balls appeared in the images as 5 to 7 pixels in diameter.

Twelve well-distributed ground control points (GCPs) were established on the surrounding stable trees. The 3D coordinates of the GCPs were measured with a Leica TCR407 Power reflectorless total station with a standard deviation of $\pm 2 \cdot 0$ mm in the X and Y coordinates and $\pm 1 \cdot 0$ mm in Z.

The GCPs and the balls were illuminated using strong halogen lamps during the night-time. The radiometric settings (brightness, contrast, gain and exposure time) of the cameras were adjusted periodically for daytime and night-time exposure by the in-house image acquisition software. The same software was also used for automatic shooting and storing of the images.

Calibration and Orientation

A laboratory testfield calibration was performed on the cameras and their configuration. The photogrammetric 3D calibration field at the Institute of Geodesy and Photogrammetry at ETH Zurich was used (Akca and Gruen, 2009). It is $3 \cdot 4$ m $\times$ $2 \cdot 0$ m $\times$ $1 \cdot 0$ m in size (Fig. 8). The room has a stable temperature (22°C) and humidity (40%) by means of air conditioning. The 3D coordinates of 87 well-distributed control points were measured using a Leica Axyz system. The average theoretical precision values of the control points was

FIG. 8. The photogrammetric 3D calibration field at the Institute of Geodesy and Photogrammetry at ETH Zurich. The picture was taken by CAM1.
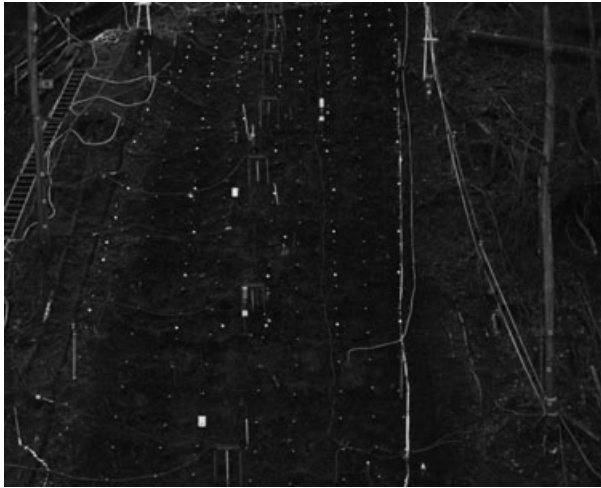
Fɪɢ. 9. An image taken from CAM3 in the evening at 6:00:00 p.m. The larger white spots are the tennis balls used in this paper (the smaller white spots are part of a separate experiment).

±0·03, ±0·05 and ±0·03 mm for the *X*, *Y* and *Z* axes, respectively. Note that the *Y* axis is the depth direction here.

For each of the four cameras, nine images were taken (from three different horizontal positions, each combined with three different vertical positions) in a convergent geometry mode. Six images were taken in normal mode and the remaining three images were rotated in order to de-correlate the interior and exterior orientation parameters.

All tie point and control point measurements were carried out interactively using the least squares image matching method implemented in the BAAP software. BAAP is a GUI-based MS Windows software package, specifically designed for close range photogrammetric applications (Akca and Gruen, 2009). It was developed (in-house) using the C++ Builder 5·0 integrated development environment (IDE).

The self-calibrating bundle adjustment, implemented in the SGAP software, was used for the final estimation of the parameters. SGAP software has a command-line interface and offers sophisticated photogrammetric bundle adjustment modules. It has been developed at the Institute of Geodesy and Photogrammetry at ETH Zurich (Beyer, 1992).

The average standard deviation of image point observations $\hat{\sigma}_0$ is 0·36 μm, which translates to 1/13 of a pixel of the CCD sensors. Part of the calibration results are given in Table II. Columns *STD-X*, *STD-Y* and *STD-Z* give the average theoretical precision values of tie points for the respective cameras. The best relative in-plane precision of 1:22 000 and 0·0066% of average depth was achieved for CAM1.

The estimated additional parameters (APs) are given in Table III. In all cases, the remaining APs (K_2 and K_3 coefficients of the radial distortion, affinity, shear, P_1 and P_2 coefficients of tangential distortion) were excluded from the bundle adjustment due to statistical significance and determinability problems. The small values of the theoretical precisions and algebraic correlations (less than 0·41 in all cases) of APs indicate the stability of the computations.

The estimated camera calibration parameters were considered as constant over time in the subsequent point positioning computations. Since the camera stations on two tall trees

TABLE II. Results of the 3D testfield camera calibration.

Camera name	Principal distance (mm)	$\hat{\sigma}_0$ (μm)	STD-X (mm)	STD-Y (mm)	STD-Z (mm)
CAM1	8·286 ± 0·001	0·40	0·14	0·33	0·11
CAM2	8·296 ± 0·001	0·35	0·14	0·36	0·12
CAM3	12·047 ± 0·001	0·34	0·22	0·48	0·15
CAM4	12·075 ± 0·001	0·34	0·19	0·33	0·13
Mean		0·36	0·17	0·38	0·13

STD-X: average theoretical precision values of tie points along the *X* axis. Similarly for *Y* and *Z*.

TABLE III. Estimated additional parameters.

Camera name	x_0 (mm)	y_0 (mm)	K_1
CAM1	−0·026 ± 0·001	−0·155 ± 0·001	−8·775E−004 ± 3·918E−006
CAM2	0·079 ± 0·001	−0·175 ± 0·001	−8·772E−004 ± 4·493E−006
CAM3	0·040 ± 0·001	0·066 ± 0·001	−2·756E−004 ± 3·695E−006
CAM4	0·122 ± 0·001	0·098 ± 0·001	−1·896E−004 ± 3·154E−006

were not stable platforms and were moving with the wind, the exterior orientation (EO) of the cameras was calculated for each camera/image frame individually, by use of the GCPs.

Landslide during Artificial Rainfall

Image acquisition of the second sprinkling experiment started on 16th March 2009 at 3:28 p.m. and ended the next day at 11:58 a.m. The photogrammetric system worked continuously for 20 h and 30 min, and collected approximately 2·5 million grey-level images of the scene (Fig. 9). Although the cameras can provide 24-bit colour images, 8-bit grey-scale images were acquired for faster data transmission and processing purposes.

With the properly aligned sprinklers, the artificial rainfall was adjusted to an average distribution of 15 mm/h. Uniform sprinkling was achieved with 360° spray nozzles. Due to the high infiltration capacity, the fine mist penetrated into the soil quickly. Thus, very little surface runoff occurred during the experiment.

There was an instant response in the upper part of the test area as the degree of saturation increased, absorption dropped and then the water table rose over 5 h to about 1·5 m below ground level, where it stayed for the next 10 h. Fifteen hours after the rainfall had begun, at 3:00 a.m., the upper right quadrant started to creep downhill, with the rate increasing until 3:23 a.m. (Figs. 10, 11 and 12). It took 36 s to mobilise about 130 m³ of soil and roots, which travelled on a slightly leftward trajectory towards a tree stump in the lower part of the field, which re-directed the flow and caused it to accelerate towards the bottom right, whereupon it took only 12 s more to impact on the protection net (Springman et al., 2010).

Processing the Imagery

Post-processing, Target Tracking and Point Positioning

The images were processed in three temporal frequency groups:

(1) *Hour-by-hour (1 fph)*: 1 frame per hour starting from 6:00 p.m. until 3:00 a.m., totalling 8 epochs and 8 × 4 = 32 images.
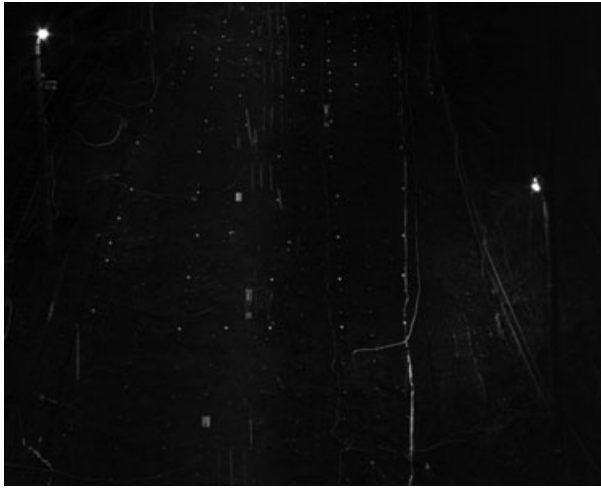
FIG. 10. A CAM3 image just before the landslide at 3:23:00 a.m.

FIG. 11. A CAM3 image just after the landslide at 3:24:18 a.m.

(2) *Minute-by-minute (1 fpm)*: 1 frame per minute starting from 3:01 a.m. until 3:23 a.m., totalling 23 epochs and 23 × 4 = 92 images.
(3) *Original imaging frequency (5 fps)*: 5 frames per second starting from 3:23:00·000 a.m. until 3:24:00·909 a.m., totalling 263 epochs and 263 × 4 = 1052 images.

The cameras were set to operate at 10 fps through the control software. However, in practice an average image acquisition speed of 8 fps during the daytime and 5 fps during the night-time was achieved. This deficiency was reported to IDS, but no satisfactory explanation (and solution) could be given.

Fig. 12. A CAM3 image in the morning at 7:00:00 a.m.

All image measurements were performed automatically using an image tracking algorithm implemented as a module inside the BAAP software.

During an initialisation step, the tennis balls were measured semi-automatically using only the four 6:00 p.m. images of the 1 fph group, using cross-correlation template matching. The template image is a white circle that is generated artificially on a black background, and is 11×11 pixels in size (Fig. 13). In this step, the initial positions of the targets are provided by the operator. Then, the tracking algorithm automatically searches for the template image in the next frames, in a recursive procedure. The 11×11 pixel cross-correlation window seeks the sub-pixel matching location inside a circular search area of 15 pixels in radius. The origin of the circular search area is defined by the pixel coordinates given in the previous frame. If the cross-correlation coefficient sinks below 0·85 for any point, this point is excluded from being tracked in subsequent frames. Such points are lost mainly due to occlusions or to the balls "jumping" away due to the landslide.

The tracking algorithm produced satisfactory results. Only 4% of the resulting image measurements were erroneous. All erroneous cases occurred in the 5 fps computations when the landslide had been triggered. Fig. 14 shows an example where point 33 has been lost in the last frame. The point was obscured by another object here. The tracking algorithm finds
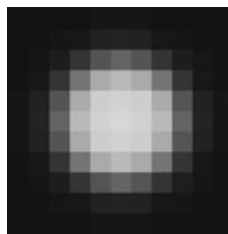

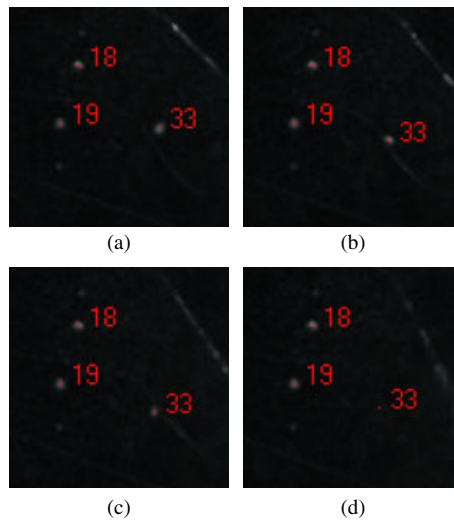Fig. 13. The template image is 11×11 pixels in size.

Fig. 14. Four consecutive frames of CAM1 during the landslide activity. The images are enlarged 3 times for visualisation purposes. Tennis ball 33 has been lost in the last frame.

an erroneous location for point 33 whose cross-correlation coefficient is less than the threshold limit (0·85). This point was then excluded in the subsequent frames.

Although the network configuration gave 100% imaging overlap for all four cameras, the field instruments (for example, sprinklers, deformation probes and acoustic sensors) obscured a few of the tennis balls. Eight of the total of 63 tennis balls (13%) were only visible from three of the cameras; the remaining 55 tennis balls (87%) were captured by all four cameras. In total, $(8 - 1) + 23 + 263 = 293$ images (or epochs) were measured automatically for each camera. This procedure was repeated for the image sets of all four cameras.

The image measurements generated (together with their ancillary data) were input into the SGAP software. The SGAP software computed 294 individual bundle adjustments in batch computation mode. The average sigma naught (σ_0) of the all computations is 0·43 µm, which is equal to 1/11 of a pixel of the imaging system (Table IV). The mean theoretical precisions of the estimated coordinates of the tennis balls are $\pm 16·9$ mm along the horizontal plane and $\pm 6·5$ mm in the vertical direction. The precision achieved is in close agreement with the simulation results and the project requirements. Note that these numbers are one σ values, which accounts for only 68% of the errors falling into this range. The relative

TABLE IV. Theoretical point positioning precisions of the tennis balls.

Groups	$\hat{\sigma}_0$ (µm)	STD-X (mm)	STD-Y (mm)	STD-Z (mm)
1 fph	0·45	7·0	15·5	6·6
1 fpm	0·43	7·0	15·4	6·5
5 fps	0·41	7·0	15·4	6·3
Mean	0·43	7·0	15·4	6·5

precision values can be computed considering the size of the test site and average depth, which are 1:5000 in-plane and 0·03% of depth.

The computation took 26 minutes on a high-end desktop computer. In a typical bundle adjustment of 1 fph and 1 fpm computations where any tracking point has not been lost, the following structure is observed:

(1) Data definition: 4 images; 4 APs (fixed); 63 object points; 10 GCPs (fixed).
(2) Observations: 504 image point observations.
(3) Unknowns: 189 object point coordinates; 24 EO parameters.
(4) Degrees of freedom: 291.

Outliers were automatically identified and localised with a two-level strategy:

(1) The limit of the cross-correlation coefficient set as 0·85 in the tracking algorithm run by the BAAP software.
(2) Outlier test in the batch mode bundle adjustments run by the SGAP software.

Once located, each outlier was inspected and corrected interactively.

The relative displacements along the horizontal and vertical directions are illustrated graphically in Figs. 15 and 16. The displacements were computed by subtracting the X, Y, Z coordinate values of the subsequent frames on a point basis. A similar comparison can also be performed in the surface domain (Gruen and Akca, 2005; Akca, 2010; Akca et al., 2010).
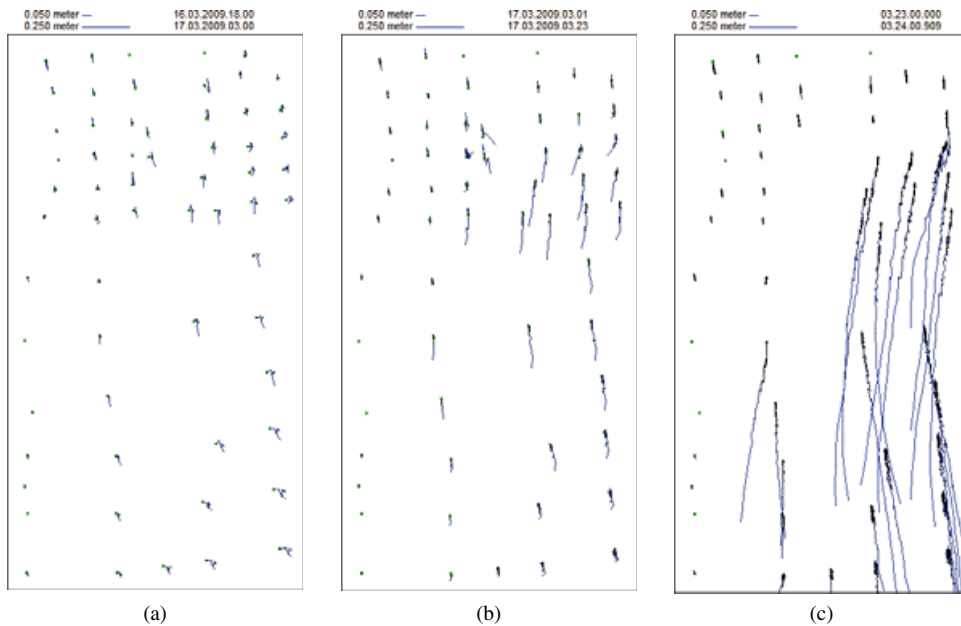

Fig. 15. Horizontal displacement of the tennis balls: (a) 1 fph between 6:00 p.m. and 3:00 a.m.; (b) 1 fpm between 3:01 a.m. and 3:23 a.m.; and (c) 5 fps between 3:23:00 a.m. and 3:24:00 a.m.
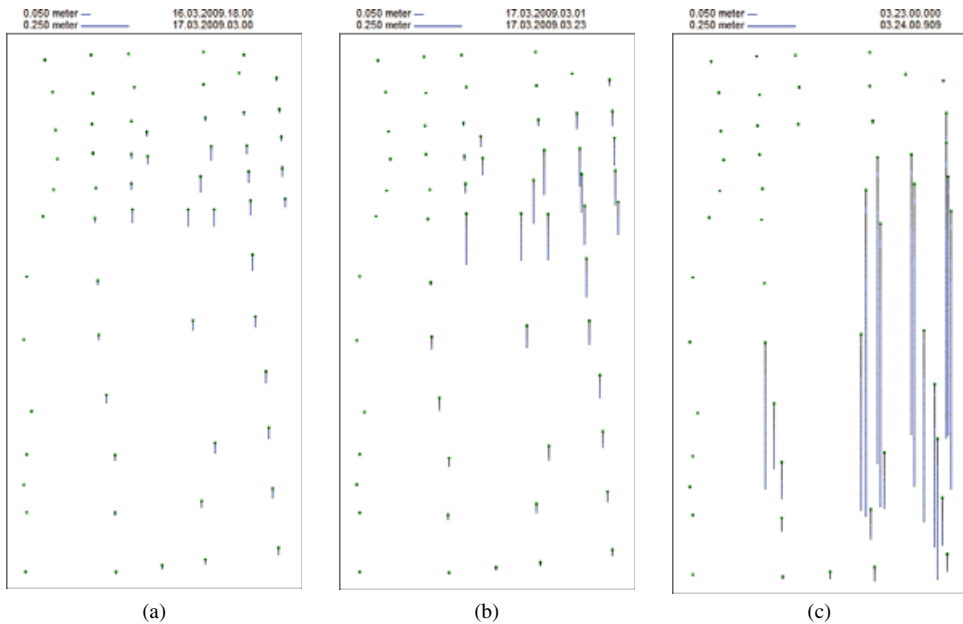
FIG. 16. Vertical displacement of the tennis balls in the same timeframes as Fig. 15: (a) 1 fph; (b) 1 fpm; and (c) 5 fps.

From 6:00 p.m. until 3:00 a.m., the 1 fph computations show relatively small planar movements both down the slope and across the slope (Fig. 15(a)).

At 9:00 p.m. the surface of the upper half of the area was raised by 1 to 3 cm. This instant represents the extreme upward movement of the surface. Between 9:00 p.m. and 1:00 a.m. the vertical movement gradually decreased. In the next hour, at 2:00 a.m., the vertical movement suddenly changed to a downward direction, starting to lower by 2 to 4 cm. At 3:00 a.m., the right half of the field was lowered by 4 to 6 cm (Fig. 16(a)). The slope kept its steady state during the 12-hour period from the start of sprinkling at 3:00 p.m. until this moment.

Between 3:01 a.m. and 3:23 a.m., the upper right quadrant started to move down the slope in slow motion; at some points this movement totalled 40 cm in the horizontal plane (Fig. 15(b)) and 30 cm in the vertical direction (Fig. 16(b)). The velocity was 3·0 cm/min on average and 11·8 cm/min at its maximum.

The landslide occurred between 3:23 a.m. and 3:24 a.m., lasting 48 seconds. In this time span, the upper right quadrant flowed along the slope with an average velocity of 14·0 cm/s, and a maximum speed of 100·4 cm/s was reached at some locations (Figs. 15 (c) and 16(c)).

The wooden sticks fixed to the tennis balls have a depth of 20 to 25 cm into the ground. They are used as targets and not as tracers on the surface that would represent debris particles in size or weight. The tennis balls are controlled by differential movements of 20 to 25 cm thick debris packages. The 3D movements are assumed to follow the landslide direction. Occasionally, 3D movements may point in any direction rather than downhill. Even the size and installation of the wooden sticks may influence the observed

movement, but these small perturbations are relatively minor and should not affect the results significantly.

<div align="center">Conclusions</div>

The Ruedlingen experiment is a sub-project within the framework of the TRAMM project. The express purpose was to trigger a rainfall-induced landslide, having exposed the slope to continuous observation using high-resolution cameras. A photogrammetric network was designed and installed, given that photogrammetry is a cost-effective and accurate method for such tasks. In the experiment the photogrammetric monitoring system has a cost of CHF 13 000 including cameras, lenses, protection cases, NIC card and cables. The intellectual property of the software packages developed has to be considered separately.

Planning and designing are the key steps when environmental conditions and project specifications have strict limitations. The simulations, performed by the in-house developed PanCam routine, aided the design stage. Different photogrammetric network options were simulated; the optimal one was chosen by considering the project requirements and the budget. In this way, during the early stages of the project, the output and final computational requirements could be predicted and the hardware was purchased accordingly.

Based on the simulation results, four IDS cameras with 1280×1024 CCD sensors were used. Although the factory specifications of the IDS cameras report a 14 fps image acquisition rate, only a 5 to 8 fps acquisition rate was achieved during the experiments. Nevertheless, the results of the photogrammetric processing fulfilled the project requirements, largely because the landslide developed over a long period of time compared with an earlier example in Japan (Ochiai et al., 2004) which had failed and flowed within about 5 seconds.

The surface deformation was quantified by tracking the small tennis balls pegged into the ground, achieving an average 3D point positioning precision of $\pm 1 \cdot 8$ cm. The results of the photogrammetric work provide a better understanding of the surface dynamics of landslides.

<div align="center">Acknowledgements</div>

<div align="center">REFERENCES</div>

AKCA, D., 2010. Co-registration of surfaces by 3D least squares matching. *Photogrammetric Engineering & Remote Sensing*, 76(3): 307–318.

AKCA, D. and GRUEN, A., 2009. Comparative geometric and radiometric evaluation of mobile phone and still video cameras. *Photogrammetric Record*, 24(127): 217–245.

AKCA, D., FREEMAN, M., SARGENT, I. and GRUEN, A., 2010. Quality assessment of 3D building data. *Photogrammetric Record*, 25(132): 339–355.

AKCA, D., GRUEN, A., ASKARINEJAD, A. and SPRINGMAN, S. M., 2011. Photogrammetric monitoring of an artificially generated landslide. *International Conference on GeoInformation for Disaster Management*, Antalya, Turkey. 10 pages (on CD-ROM).

AMIRI PARIAN, J., GRUEN, A. and COZZANI, A., 2007. Monitoring of the reflectors of ESA's Planck telescope by close-range photogrammetry. *Journal of Applied Geodesy*, 1(3): 137–145.

ANGELI, M.-G., PASUTO, A. and SILVANO, S., 2000. A critical review of landslide monitoring experiences. *Engineering Geology*, 55(3): 133–147.

ASKARINEJAD, A., CASINI, F., KIENZLER, P., TEYSSEIRE, P. and SPRINGMAN, S. M., 2010. Mountain risks: two case histories of landslides induced by artificial rainfall on steep slopes. *International Conference on Mountain Risks: Bringing Science to Society*, Florence, Italy. 437 pages: 201–206.

AYALEW, L., YAMAGISHI, H., MARUI, H. and KANNO, T., 2005. Landslides in Sado Island of Japan: Part I. Case studies, monitoring techniques and environmental considerations. *Engineering Geology*, 81(4): 419–431.

BALDI, P., CENNI, N., FABRIS, M. and ZANUTTA, A., 2008. Kinematics of a landslide derived from archival photogrammetry and GPS data. *Geomorphology*, 102(3–4): 435–444.

BELL, R., PETSCHKO, H., RÖHRS, M. and DIX, A., 2012. Assessment of landslide age, landslide persistence and human impact using airborne laser scanning digital terrain models. *Geografiska Annaler: Series A, Physical Geography*, 94(1): 135–156.

BEYER, H. A., 1992. *Geometric and radiometric analysis of a CCD-camera based photogrammetric close-range system*. Mitteilungen Nr. 51, Institute for Geodesy and Photogrammetry, ETH Zurich, Switzerland. 186 pages.

CHADWICK, J., DORSCH, S., GLENN, N., THACKRAY, G. and SHILLING, K., 2005. Application of multi-temporal high-resolution imagery and GPS in a study of the motion of a canyon rim landslide. *ISPRS Journal of Photogrammetry and Remote Sensing*, 59(4): 212–221.

CORSINI, A., PASUTO, A., SOLDATI, M. and ZANNONI, A., 2005. Field monitoring of the Corvara landslide (Dolomites, Italy) and its relevance for hazard assessment. *Geomorphology*, 66(1–4): 149–165.

DEBELLA-GILO, M. and KÄÄB, A., 2012. Measurement of surface displacement and deformation of mass movements using least squares matching of repeat high resolution satellite and aerial images. *Remote Sensing*, 4(1): 43–67.

DEWEZ, T., NACHBAUR, A., MATHON, C., SEDAN, O., KOBAYASHI, C., HIBERT, C., BERGER, F., DES GARETS, E. and NOWAK, E., 2010. OFAI: 3D block tracking for a real-size rockfall experiment in the weathered volcanic context of Tahiti, French Polynesia. *International Symposium on the Rock Slope Stability*, Paris, France. 13 pages (on CD-ROM).

DEWITTE, O., JASSELETTE, J.-C., CORNET, Y., VAN DEN EECKHAUT, M., COLLIGNON, A., POESEN, J. and DEMOULIN, A., 2008. Tracking landslide displacements by multi-temporal DTMs: a combined aerial stereophotogrammetric and LIDAR approach in western Belgium. *Engineering Geology*, 99(1–2): 11–22.

GRUEN, A. and AKCA, D., 2005. Least squares 3D surface and curve matching. *ISPRS Journal of Photogrammetry and Remote Sensing*, 59(3): 151–174.

LODHI, M. A., 2011. Earthquake-induced landslide mapping in the western Himalayas using medium resolution ASTER imagery. *International Journal of Remote Sensing*, 32(19): 5331–5346.

MALET, J.-P., MAQUAIRE, O. and CALAIS, E., 2002. The use of Global Positioning System techniques for the continuous monitoring of landslides: application to the Super-Sauze earthflow (Alpes-de-Haute-Provence, France). *Geomorphology*, 43(1–2): 33–54.

MARTHA, T. R., KERLE, N., JETTEN, V., VAN WESTEN, C. J. and KUMAR, K. V., 2010. Landslide volumetric analysis using Cartosat-1-derived DEMs. *IEEE Geoscience and Remote Sensing Letters*, 7(3): 582–586.

METTERNICHT, G., HURNI, L. and GOGU, R., 2005. Remote sensing of landslides: an analysis of the potential contribution to geo-spatial systems for hazard assessment in mountainous environments. *Remote Sensing of Environment*, 98(2–3): 284–303.

MORA, P., BALDI, P., CASULA, G., FABRIS, M., GHIROTTI, M., MAZZINI, E. and PESCI, A., 2003. Global Positioning Systems and digital photogrammetry for the monitoring of mass movements: application to the Ca' di Malta landslide (northern Apennines, Italy). *Engineering Geology*, 68(1–2): 103–121.

NIETHAMMER, U., JAMES, M. R., ROTHMUND, S., TRAVELLETTI, J. and JOSWIG, M., 2012. UAV-based remote sensing of the Super-Sauze landslide: evaluation and results. *Engineering Geology*, 128(1): 2–11.

OCHIAI, H., OKADA, Y., FURUYA, G., OKURA, Y., MATSUI, T., SAMMORI, T., TERAJIMA, T. and SASSA, K., 2004. A fluidized landslide on a natural slope by artificial rainfall. *Landslides*, 1(3): 211–219.

OLAGUE, G. and DUNN, E., 2007. Development of a practical photogrammetric network design using evolutionary computing. *Photogrammetric Record*, 22(117): 22–38.

PESCI, A., TEZA, G., CASULA, G., LODDO, F., DE MARTINO, P., DOLCE, M., OBRIZZO, F. and PINGUE, F., 2011. Multitemporal laser scanner-based observation of the Mt. Vesuvius crater: characterization of overall geometry and recognition of landslide events. *ISPRS Journal of Photogrammetry and Remote Sensing*, 66(3): 327–336.

PETLEY, D. N., MANTOVANI, F., BULMER, M. H. and ZANNONI, A., 2005. The use of surface monitoring data for the interpretation of landslide movement patterns. *Geomorphology*, 66(1–4): 133–147.

RIEKE-ZAPP, D. H., ROSENBAUER, R. and SCHLUNEGGER, F., 2009. A photogrammetric surveying method for field applications. *Photogrammetric Record*, 24(125): 5–22.

SAADATSERESHT, M., FRASER, C. S., SAMADZADEGAN, F. and AZIZI, A., 2004. Visibility analysis in vision metrology network design. *Photogrammetric Record*, 19(107): 219–236.

SPRINGMAN, S., ASKARINEJAD, A., KIENZLER, P., CASINI, F., SPERL, M., BLEIKER, E., AKCA, D. and GRUEN, A., 2010. The Ruedlingen monitoring and landslide experiment. *D-BAUG Annual Report 2009*, Department of Civil, Environmental and Geomatic Engineering, ETH Zurich, Switzerland. 84 pages: 26–31. http://www.baug.ethz.ch/about/annual_reports/baug_report_2009.pdf [Accessed: 20th April 2012].

TARCHI, D., CASAGLI, N., FANTI, R., LEVA, D. D., LUZI, G., PASUTO, A., PIERACCINI, M. and SILVANO, S., 2003. Landslide monitoring by using ground-based SAR interferometry: an example of application to the Tessina landslide in Italy. *Engineering Geology*, 68(1–2): 15–30.

TRAVELLETTI, J., OPPIKOFER, T., DELACOURT, C., MALET, J.-P. and JABOYEDOFF, M., 2008. Monitoring landslide displacements during a controlled rain experiment using a long-range terrestrial laser scanning (TLS). *International Archives of Photogrammetry, Remote Sensing and Spatial Information Sciences*, 37(B5): 485–490.

Résumé

Une pluie artificielle a été déversée sur un versant boisé de Ruedlingen, au nord de la Suisse. Cette expérience a déclenché un glissement de terrain, mobilisant environ 130 m^3 de matière. Le phénomène a été observé par un réseau photogrammétrique de 4 caméras à la cadence de 5 à 8 images par seconde afin de quantifier les changements spatiaux et temporels, en suivant des balles de tennis fixées au sol. Des mesures ont été effectuées dans les images en utilisant des méthodes automatiques d'appariement d'images développées dans le cadre d'un logiciel maison. L'estimation des coordonnées 3D des cibles au moyen d'une compensation par faisceaux adaptée conduit à une exactitude de localisation de ±1,8 cm.

Zusammenfassung

Ein bewaldeter Hang in Rüdlingen in der nördlichen Schweiz wurde einem künstlich erzeugten Regen ausgesetzt. Dadurch wurde ein Erdrutsch ausgelöst, der ca. 130 m^3 Geröll in Bewegung setzte. Dieses Ereignis wurde durch ein photogrammetrisches Netzwerk aus vier Kameras mit einer Aufnahmerate von 5 bis 8 Aufnahmen pro Sekunde aufgezeichnet. Zur Quantifizierung der räumlichen und zeitlichen Veränderungen wurden kleine Tennisbälle verfolgt, die in die Erde gesteckt waren. Die Messungen in den Bildern wurden durch eigens entwickelte automatische Bildzuordnungsmethoden durchgeführt. Die 3D Koordinaten der Zielpunkte wurden durch eine auf diese Anwendung adaptierte Bündelausgleichung bestimmt, womit eine Präzision der Position von ±1·8 cm erzielt werden konnte.

Resumen

Una pendiente arbolada en Ruedlingen, norte de Suiza, fue expuesta a una lluvia artificial. El experimento provoco un corrimiento de tierras el cual desplazó alrededor de 130 m^3 de escombros. El suceso fue monitorizado por una red fotogramétrica de cuatro cámaras, disparando entre 5 y 8 imágenes por segundo, para cuantificar los cambios espaciales y temporales mediante el seguimiento de pequeñas bolas (de tenis) sujetas al suelo. Las medidas en las imágenes se han realizado usando métodos automáticos de correspondencia de imágenes, implementados en un paquete de software de desarrollo propio. Las coordenadas 3D de las dianas se han estimado con un ajuste de haces a modificad0, alcanzando una exactitud de 1,8 cm en posición.

195